

pH Effects on the Molecular Structure of β -Lactoglobulin Modified Air–Water Interfaces and Its Impact on Foam Rheology

Kathrin Engelhardt,[†] Meike Lexis,[‡] Georgi Gochev,^{§,||} Christoph Konnerth,[†] Reinhard Miller,[§] Norbert Willenbacher,[‡] Wolfgang Peukert,[†] and Björn Braunschweig^{†,*}

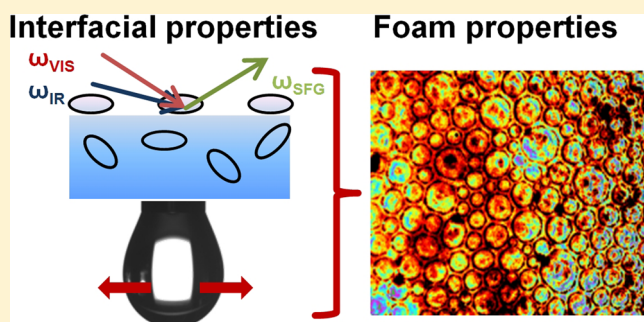
[†]Institute of Particle Technology (LFG), University of Erlangen-Nuremberg, Cauerstrasse 4, 91058 Erlangen, Germany

[‡]Institute of Mechanical Engineering, Karlsruhe Institute of Technology (KIT), Gotthard-Franz-Strasse 3, 76131 Karlsruhe, Germany

[§]Max-Planck-Institute of Colloids and Interfaces, Am Mühlenberg 1, 14476 Potsdam, Germany

^{||}Institute of Physical Chemistry, Bulgarian Academy of Sciences, 1113 Sofia, Bulgaria

ABSTRACT: Macroscopic properties of aqueous β -lactoglobulin (BLG) foams and the molecular properties of BLG modified air–water interfaces as their major structural element were investigated with a unique combination of foam rheology measurements and interfacial sensitive methods such as sum-frequency generation and interfacial dilatational rheology. The molecular structure and protein–protein interactions at the air–water interface can be changed substantially with the solution pH and result in major changes in interfacial dilatational and foam rheology. At a pH near the interfacial isoelectric point BLG molecules carry zero net charge and disordered multilayers with the highest interfacial dilatational elasticity are formed at the air–water interface. Increasing or decreasing the pH with respect to the isoelectric point leads to the formation of a BLG monolayer with repulsive electrostatic interactions among the adsorbed molecules which decrease the interfacial dilatational elasticity. The latter molecular information does explain the behavior of BLG foams in our rheological studies, where in fact the highest apparent yield stresses and storage moduli are established with foams from electrolyte solutions with a pH close to the isoelectric point of BLG. At this pH the gas bubbles of the foam are stabilized by BLG multilayers with attractive intermolecular interactions at the ubiquitous air–water interfaces, while BLG layers with repulsive interactions decrease the apparent yield stress and storage moduli as stabilization of gas bubbles with a monolayer of BLG is less effective.



1. INTRODUCTION

Foams as dispersions of gases in liquids show unique rheological properties: Under the application of comparatively small stresses they behave like a viscoelastic solid, while at higher stresses they become shear thinning and flow like a liquid. This mechanical behavior of foams in combination with a remarkably high surface area and low density leads to a variety of demanding applications.^{1,2} Among the latter, protein foams that are present in dairy products^{3–5} are in particular interesting since the physical and chemical properties of the inherent air–water interfaces largely determine the macroscopic properties of the foam.⁶ As air–water interfaces are a basic structure element of aqueous foams, they can control foam rheology and other macroscopic properties such as foam stability.^{7,8} For that reason it is of great importance to increase our level of understanding of protein adsorption and stabilization mechanisms at the interface of a foam lamella. The latter information would help to control and to tune foam properties such as foamability, foam stability, or mechanical properties of the macroscopic foam. In general, in situ molecular level studies of protein adsorption are needed to address changes in the

composition and molecular structure of protein adsorption layers at the air–water interface directly.

In the past, protein interfaces were studied with techniques such as ellipsometry,⁹ neutron reflection,^{10,11} X-ray reflectivity,¹² Brewster angle microscopy,¹³ and with surface tension measurements.^{14,15} However, in recent years vibrational sum-frequency generation (SFG) has become a powerful tool for surface science studies of biointerfaces.^{6,16–23}

In this article we report the use of a combination of established analytical techniques such as bubble profile analysis tensiometry, surface dilatational rheology, ellipsometry, and foam rheology measurements with vibrational SFG spectroscopy. This unique approach allows us to address not only single properties of foams or interfaces but also provides information on several length scales. As we will demonstrate the latter approach has enabled us to reveal composition, structure, and mechanical properties of β -lactoglobulin (BLG) interfacial

Received: July 18, 2013

Revised: August 19, 2013

layers and foams and thus to bridge the gap between the molecular level and the macroscopic aqueous foam.

2. EXPERIMENTAL DETAILS

2.1. Sample Preparation. BLG was isolated as described previously²⁴ and kindly provided by the group of Ulrich Kulozik (Technische Universität München, Germany). BLG solutions were prepared by dissolving the dry protein in ultrapure water (18.2 MΩ·cm; total oxidizable carbon <5 ppb). The pH was adjusted by adding either HCl or NaOH (Merck; Suprapur grade or Carl Roth 1 N standard solution K021) and, subsequently, measured with a pH electrode. In order to remove possible organic contaminations, the necessary glassware for spectroscopic studies was soaked in a mixture of concentrated sulfuric acid (98%; analytical grade) and NOCHROMIX for at least 24 h and was subsequently thoroughly rinsed with ultrapure water. All measurements were performed at room temperature. The foams were produced by purging nitrogen (60 mL/min) through a porous glass filter (pore size 9–16 μm) that was fused to a glass pipe of 60 mm diameter and 53 mm height, while the sample solution was placed on top of this filter. The protein solutions were previously heated to 50 °C in order to obtain foams that are stable enough for reproducible rheological measurements. This temperature treatment only increases the adsorption kinetics but also is still low enough to exclude denaturation of BLG. In fact, BLG is being denatured between 70 and 85 °C.²⁵

2.2. Zeta Potential Measurements. Zeta potentials were measured with a Zetasizer Nano ZS from Malvern Instruments. With the Zetasizer Nano ZS reproducible zeta potentials of BLG could only be recorded for concentrations >546 μM. Therefore, higher BLG concentrations had to be chosen for measurements of the bulk zeta potential compared to the measurements at the air–water interface. Before the solution was transferred into the cuvettes for zeta potential measurements, BLG dilutions are filtered with a 0.2 μm cellulose acetate filter (VWR 514-0060) and a thoroughly acid cleaned glass syringe. For each pH value at least five measurements with different cuvettes were performed.

2.3. Bubble Shape Analysis. Surface tensions σ of protein modified air–water interfaces were determined with drop/bubble profile analysis²⁶ using a PAT-1 tensiometer (SINTERFACE Technologies, Germany). The variation of the Laplacian shape of an emerging bubble with a constant volume of 12 μL in the protein solution was measured as a function of adsorption time and was used to determine the dynamic surface tension. The establishment of equilibrium surface tension of protein solutions is a continuous process, which has been analyzed by a quasi-equilibrium state approach.^{27,28} In this study we chose a reference adsorption time of 30 min, during which a sufficiently high surface saturation was ensured for the two BLG concentrations measured. In order to monitor the surface dilational rheological properties of the adsorbed layer, sinusoidal oscillations with 10% amplitude with respect to the bubble area and a frequency of 0.1 Hz were applied, and the response in surface tension was recorded. The experimental data were processed for the surface dilational viscoelastic modulus $E = E' + E''$, whereby E' the storage and E'' the loss moduli account respectively for the dilational elasticity and dilational viscosity of an adsorption layer.²⁹

2.4. Ellipsometry. The thickness of adsorbed protein layers was determined with a phase modulated ellipsometer (Beaglehole Instruments, Picometer ellipsometer) that was operated with a wavelength of 632.8 nm. For each experiment 15 μM BLG sample solution was poured into a Petri dish with a diameter of 10 cm and was allowed to equilibrate for about 30 min. Angle scans between 51° and 55° vs the surface normal were performed with a step width of 0.5°. In order to ensure reproducibility, at least six measurements were recorded and averaged for every pH value. Angle-resolved data from ellipsometry were fitted using a three-layer model with refractive indices of 1.33, 1.40, and 1.00 for the electrolyte subphase, the protein layer, and air, respectively. In general two parameters are unknown in this three-layer system: the layer thickness of the adsorbed protein layer and the corresponding refractive index. Because of the fact that

these parameters cannot be determined independently, one of them—in our case the refractive index—has to be chosen as a fixed input parameter for all model calculations. The assumption of $n = 1.40$ for the protein layer is in accordance with reported layer thicknesses of around 3–4 nm for a BLG layer at pH 6–7,^{11,30} which is comparable to the diameter of a BLG monomer of around 3.6 nm.^{31,32} Since the refractive index of BLG at an interface is a priori unknown, the assumption of a fixed value for the refractive index causes a systematic error of the layer thickness that depends on the deviation of the assumed refractive index from its actual value. However, since we compare only relative changes of the layer thickness as a function of the solution pH, our interpretations are not impaired in this respect.

2.5. Vibrational Sum-Frequency Generation (SFG). SFG is a second-order nonlinear optical process³³ and is inherently interfacial specific for materials with inversion symmetry such as liquids and gases in the time average. For SFG spectroscopy two laser beams, one with a fixed wavelength (vis) and another with tunable infrared (IR) wavelength, are combined at the interface of interest, where the sum frequency of the two impinging laser fields is generated. The intensity of sum-frequency output I_{SF} depends on the intensities of the impinging laser beams as well as on the nonresonant $\chi_{\text{NR}}^{(2)}$ and resonant parts of the second-order nonlinear susceptibility $\chi^{(2)}$:

$$I_{\text{SF}}(\omega_{\text{SF}}) \propto \left| \chi_{\text{NR}}^{(2)} + \sum_k \frac{A_k \exp(i\varphi_k)}{\omega_k - \omega + i\Gamma_k} \right|^2 I_{\text{VIS}} I_{\text{IR}} \quad (1)$$

The resonant contribution is a function of the oscillator strength $A_k = N\langle\alpha_k\mu_k\rangle$, the relative phase φ_k , the resonance frequency ω_k , and of the bandwidth Γ_k of the vibrational mode k . Furthermore, A_k depends on the number density N of the molecular species which gives rise to the vibrational mode k , and due to the coherent process of sum-frequency generation, A_k is an orientational average of the Raman polarizability α_k and the dynamic dipole moment μ_k . This orientational average can have a dramatic effect on the SFG intensity because only a perfectly ordered adsorption layer results in the highest possible SFG intensity, while a layer with identical coverage, but randomly oriented interfacial molecules, has a negligible SFG intensity. Consequently, SFG is sensitive not only to changes in the adsorbate composition and coverage at the interface but also to the inherent molecular order of the adsorbate layer.

Our SFG measurements were performed with a home built broadband SFG spectrometer that is described elsewhere.³⁴ The spectrometer is equipped with a tunable femtosecond IR laser (fwhm bandwidth >200 cm⁻¹) and an etalon filtered pulse at 800 nm wavelength (fwhm bandwidth <6 cm⁻¹). All spectra were recorded with s-polarized sum frequency, s-polarized visible, and p-polarized IR beams (ssp). The presented spectra were normalized to a reference spectrum of an oxygen plasma cleaned polycrystalline Au sample. SFG spectra were collected from 15 μM BLG solution in a Petri dish. Each spectrum was measured by scanning the broadband IR beam with a step width of 130 cm⁻¹ and a total acquisition time of 8 min for the frequency range 2800–3800 cm⁻¹.

2.6. Properties of the Protein Solutions and Foams Used for Foam Rheological Measurements. The continuous phase viscosity of foams is supposed to have an influence on their rheology.³⁵ Therefore, the viscosities of the BLG solutions were measured with the Ares rheometer from TA Instruments using concentric cylinder geometry with double gap (32/34 mm). Shear rates between 10 and 250 s⁻¹ were imposed, and the solutions showed Newtonian behavior as expected. The variation of the viscosities was negligibly low with $\eta = 0.93\text{--}1.1$ mPa·s.

The equilibrium values of the surface tension σ for the normalization of apparent foam yield stress τ_y and storage modulus G_0 were measured at 21 °C after 20 min adsorption time using the pendant drop method (Dataphysics SCA 20) (Table 1). The surface tension shows a temperature dependence that is attributable to the change of the surface tension of pure water.³⁶ It also shows a time dependence rising from the time-dependent adsorption of the proteins. Since the foams possess different temperatures and ages, an error arises in our calculations by using the equilibrium surface

Table 1. Equilibrium Surface Tension and Mean Bubble Radius at Initial and Final ϕ Used for Normalization of τ_y and G_0

pH	$\sigma/\text{mN m}^{-1}$	$r_{32}/\mu\text{m}$ (initial ϕ)	$r_{32}/\mu\text{m}$ (final ϕ)
3	47.6 ± 0.2	208 ± 12	219 ± 4
5	45.5 ± 0.4	187 ± 6	289 ± 1
6.8	51.5 ± 0.1	219 ± 3	307 ± 2

tension at 21 °C. This error can be estimated to be less than 5% which does not impair the interpretation of our results.

The gas volume fraction was determined as a function of foam age with a conductivity electrode (WTW, Cond 340i) including a temperature sensor.

The gas volume fraction ϕ can be calculated from the ratio of foam and solution conductivity κ according to the method described by Feitosa et al.³⁷

$$\phi = 1 - \frac{3\kappa(1 + 11\kappa)}{1 + 25\kappa + 10\kappa^2}$$

with $\kappa = \kappa_{\text{foam}}/\kappa_{\text{liquid}}$. The foam cools down during aging which leads to a change in the liquid conductivity κ_{liquid} with decreasing temperature. This temperature dependence was determined separately and taken into account when calculating ϕ .

Another important parameter for the rheology of disperse systems is the size distribution of the gas bubbles. Therefore, images of the bubbles were taken with the help of an endoscopic CCD camera (Lumenera LU 160; resolution 1392×1040 pixels) that was placed inside the foam. The image analysis was carried out with the software iPS (Visiometrics, Germany), and the Sauter mean radius r_{32} —the ratio between the third and the second moment of the size distribution—was extracted (Table 1).

Foam Rheology: A Rheoscope 1 (ThermoFisher, Germany) equipped with a plate–plate system with a diameter of 60 mm was used for the rheological measurements of BLG foams. The surfaces of the plates were covered with sandpaper, and the gap between the plates was set to 6 mm. Preliminary experiments confirmed that wall slip effects can be neglected with this setup. The acquisition time for all foam rheological measurements was set to 60 s in order to limit the effect of aging processes during the measurements.

Apparent foam yield stress τ_y was determined by steady shear experiments. The foams were exposed to increasing shear stresses from initial values $\tau_i = 0.1\text{--}1$ Pa to final stresses $\tau_f = 30\text{--}150$ Pa depending on foam composition. Furthermore, we have confirmed that on the time scale of our measurements the apparent yield stress is independent of the initial and final stress values as well as on the number of data points selected for a stress ramp experiment.

Amplitude sweep experiments allow for the measurement of the storage and loss modulus (G' and G'') of the foam and were performed by varying the stress amplitude at a fixed frequency $f = 1$ Hz. In the frequency range of 0.01–10 Hz the plateau value of G' at low stresses was shown to be virtually frequency independent and is henceforth named G_0 .

3. RESULTS AND DISCUSSION

The surface charge of proteins and the resulting electric double layer is determined in bulk solutions by the solution pH. At mild pH ($3 < \text{pH} < 9$) stable suspensions composed of proteins in their inherent folded structure can be formed,³⁸ whereas at extreme pH protein unfolding and denaturation has to be considered.^{39,40} As a positive or negative net charge on the protein surface gives rise to strong repulsive intermolecular interactions, protein aggregation can be prevented. At pH values around the bulk isoelectric point (IEP) where proteins carry no net charge, they tend to aggregate and are less soluble.³⁹ These examples demonstrate that charge has a tremendous effect on the physicochemical behavior of proteins.

In order to understand the more complex behavior of proteins at aqueous interfaces, we have first determined the charging of BLG proteins with zeta potential measurements, and as we will show later, these results are extremely helpful for the understanding of molecular level properties of protein layers and macroscopic properties of protein foams.

3.1. The Zeta Potential of β -Lactoglobulin. In Figure 1 the zeta potential of BLG dilutions is presented as a function of

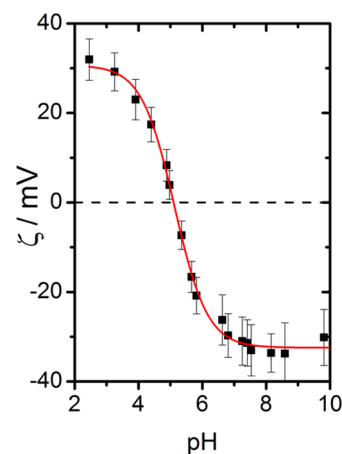


Figure 1. Zeta potential of BLG as a function of solution pH. The red line is a guide to the eye.

the solution pH. At $\text{pH} \sim 5.1$ we observe a zeta potential of 0 mV which is indicative for zero net charge and consequently for the IEP of BLG. Solution pH higher or lower compared to the IEP leads to a substantial increase in zeta potential to a maximum absolute value of 32 mV, respectively. In order to reveal the effects of protein charging on the physicochemical properties of BLG modified air–water interfaces, it is particularly interesting to compare the observed changes in zeta potential with the structure, composition, and rheological properties of the latter. Such a comparison is of great importance for the molecular level understanding of protein interfaces because interfacial properties can be significantly different from the properties of proteins in the bulk electrolyte.⁴¹ The latter is caused by local ion concentrations and pH conditions that can differ significantly from the bulk at the interface.⁴²

3.2. Surface Tension and Interfacial Dilatational Rheology of β -Lactoglobulin Layers. In a first step we have measured the surface tension and its dependence on the solution pH. In Figure 2 we compare the results for 10 and 50 μM protein concentrations. For both concentrations a pronounced minimum in surface tension is observed at a pH of ~ 5 . The minimum in surface tension at 47–50 mN/m can be attributed to an excess of BLG because the presence of proteins decreases the surface tension of the air–water interface compared to the unperturbed interface.⁴³ For both concentrations the pH at which the minimum in surface tension occurs is close to the pH of the IEP in bulk solutions. Obviously, the tendency for protein adsorption increases for pH values which are close to the IEP. Furthermore, the rate of adsorption is highest at the IEP leading to the lowest final surface tension values.⁴⁴ Consequently, the overall changes in surface tension with pH can be directly related to protein net charge effects. The highest surface activity is due to the lack of protein net charge at the IEP (Figure 1) which leads to much weaker

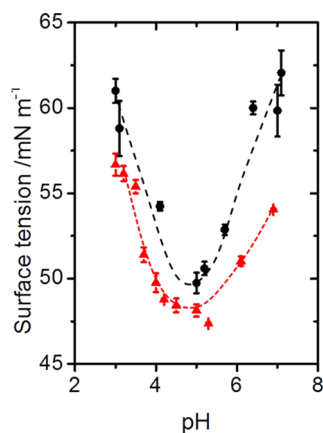


Figure 2. Surface tension for 10 (●) and 50 μM (red triangle) BLG aqueous solutions as a function of pH. Each data point corresponds to a measured value after 30 min. The dashed lines guide the eye.

repulsive interactions between the protein molecules and presumably to an increase of protein hydrophobicity.

Further insights into the intermolecular interactions of the interfacial layer can be gained by measurements of the interfacial dilational rheology of BLG adsorption layers. In Figure 3 we present the interfacial dilational elasticity E' and

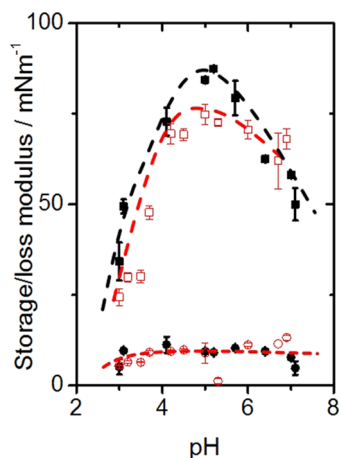


Figure 3. Interfacial dilational elasticity E' (squares) and viscosity E'' (circles) of BLG. Filled symbols correspond to a BLG concentration of 10 μM while open symbols correspond to 50 μM . The dashed lines guide the eye.

the interfacial dilational viscosity E'' as a function of the bulk pH at the same BLG concentrations as in Figure 2. A strong pH dependence of E' is observed whereby E' reaches a maximum at a pH near the bulk IEP (pH \sim 5), while E'' is an order of magnitude smaller than E' and shows virtually no pH dependence. The absence of a strong $E'' = |\text{Im} \delta|$ being the complex viscoelastic modulus,²⁹ indicates that the phase lag δ between the stress applied to the surface adsorbed protein layer and strain yield is negligible. Thus, dynamic deformations of BLG adsorption layers at the air–water interface are predominantly elastic rather than viscous.^{28,29}

The presented results in Figures 2 and 3 show that the interfacial dilational elasticity changes in accordance with the variation of the surface tension, as discussed in ref 28, exhibiting a maximum which corresponds to a minimum in the surface tension, both extremes being localized around pH 5. This

behavior is attributed to negligible electrostatic repulsive interaction which favors stronger attractive intermolecular interactions, e.g., hydrophobic interactions at the IEP. As the surface concentration is pH dependent, the formation of multilayer structures was further analyzed by ellipsometry measurements of the layer thickness and the composition and molecular order of adsorbed BLG layers with sum-frequency generation.

3.3. Composition and Structure of Surface-Adsorbed β -Lactoglobulin Layers.

In Figure 4 the thickness of BLG

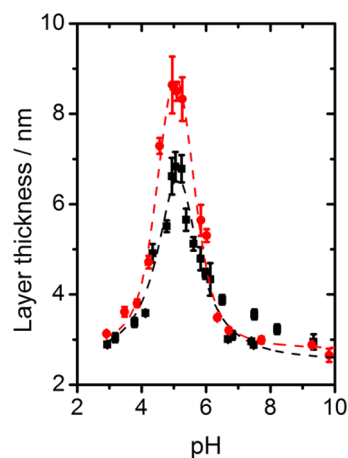


Figure 4. Thickness of BLG layers adsorbed to the air–water interface as a function of the solution pH which was determined from ellipsometry. The concentrations of BLG solutions were 15 (■) and 54 μM (red circle). The dashed lines are a guide to the eye.

layers is shown as a function of solution pH for 15 and 54 μM bulk concentrations. Similar behavior is observed for both concentrations: at acidic conditions layers with a thickness of \sim 3 nm are established, while the thickness increases with increasing pH, reaches a pronounced maximum around the bulk IEP, and decreases subsequently for higher pH values. In particular, pH values >7 result into layers with thicknesses comparable to those at acidic electrolytes with pH <4 . Here, variations of the pH had little effect on the layer thickness. Therefore, we attribute the minimum thickness which has been observed with ellipsometry to the formation of a monolayer with BLG molecules at the air–water interface. This hypothesis is corroborated by previous X-ray and neutron reflectometry studies^{11,45} of BLG at the air–water interface which have observed a thickness of \sim 3.6 nm for BLG layers. This value is close to the shortest axis of the monomer.^{31,45} On the other hand, the hydrodynamic radius of BLG molecules in solution was reported to be 2.75 ± 0.2 nm,⁴⁶ which is in a good agreement with our measured monolayer thickness of \sim 3 nm. Two possible explanations can be given for the increase in layer thickness at the bulk IEP. As we have previously discussed, the protein net charge is dramatically decreased near the IEP (Figure 1), which can lead to an accumulation of additional proteins in the adsorbed layer (Figure 2) and, consequently, to a more densely packed layer. At pH around the IEP the formation of oligomer (octamer) structures was reported.^{40,47,48} Additional multilayers could form on top of the already existing first layer, which results into a more compact protein film compared to pH conditions where only a highly charged monolayer exists at the interface. In fact, the formation of multilayers is confirmed by the thickness of proteins films at

the IEP (Figure 4) that indicates the presence of 2–3 layers of BLG at a pH of ~ 5 . Further support comes from the observed increase in storage modulus E' (Figure 3) and the decreased surface tension (Figure 2) near the IEP.

Vibrational SFG spectra of BLG proteins adsorbed to the air–water interface were recorded at different pH and provide information on the interfacial molecular structure (Figure 5a).

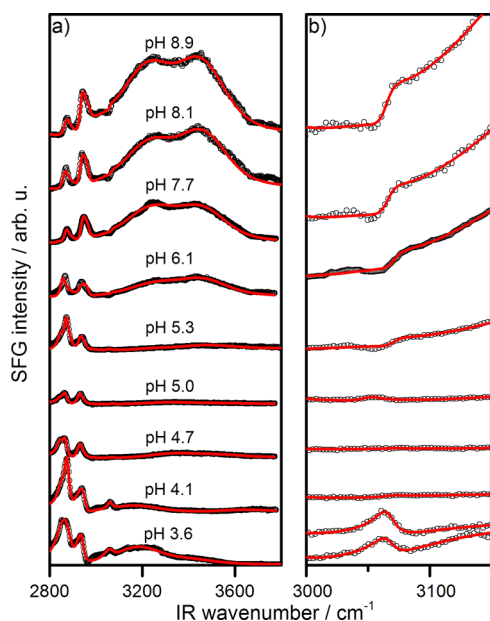


Figure 5. (a) Vibrational SFG spectra in the region of CH (2800–3100 cm^{-1}) and OH stretching vibrations (3000–3800 cm^{-1}) for BLG adsorbed to the air–water interface. Spectra were recorded at different pH as indicated in the figure. (b) Magnification of the spectra in (a) showing changes in the polarity of aromatic CH stretching band at 3050 cm^{-1} in more detail. Solid lines are fits to the experimental data according to eq 1.

In the frequency region of 2800–3100 cm^{-1} SFG spectra show strong vibrational bands centered at 2877 and 2936 cm^{-1} and a much weaker band at 3050 cm^{-1} . These bands are attributable to symmetric CH_3 stretching vibrations, the CH_3 Fermi resonance, and aromatic CH stretching vibrations of BLG proteins at the air–water interface.^{6,18,49–51} Broad vibrational bands are observed at 3200 and 3450 cm^{-1} and are due to symmetric OH stretching vibrations of tetrahedrally coordinated interfacial water molecules and molecules with lower coordination, respectively.^{52,53} The intensity of both CH and OH vibrational bands shows substantial changes when the solution pH is changed. In particular, near the bulk IEP (pH ~ 5) the intensity of OH stretching bands is close to zero while they dominate the SFG spectra at alkaline and acidic pH.

It is now interesting to discuss the origin of the observed changes in SFG intensities with variation in solution pH. We recall that the SFG amplitude $A_k \propto N \langle \alpha_k \mu_k \rangle$ is a function of both the number density and the orientational average of dynamic dipole moment and Raman polarizabilities. As we have shown before, the thickness of protein layers does increase at a pH where we observe only weak SFG contributions of all interfacial molecules. However, the number density of proteins as far as it can be deduced from the layer thickness (Figure 4) does not decrease at this point but actually increases, while the number density of interfacial water necessarily has to be similar for all pH values. For that reason the net orientation of

interfacial proteins and H_2O does dominate the SFG signals. As interfacial layers of charged proteins can create a strong unidirectional electric field E_{dc} perpendicular to the interface, interfacial dipoles such as H_2O or to some extent BLG are ordered in the electric field E_{dc} (Figure 6). This electric field induced polar ordering provides a direct dependence of the oscillator strength $A_k \propto \langle \alpha_k \mu_k \rangle$ on the local field E_{dc} .^{6,52,53}

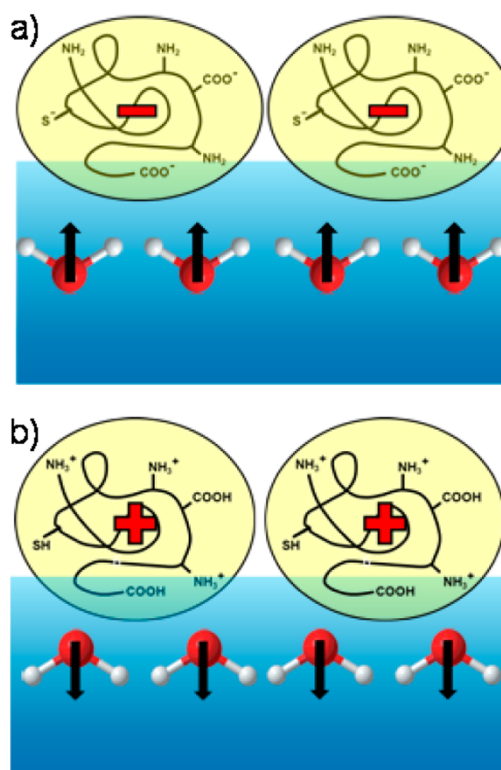


Figure 6. Simplified schematic representation of the adsorbed protein layer and the water subphase for (a) negatively charged proteins at pH below the point of zero charge and (b) positively charged proteins for a pH above the point of zero charge.

In order to analyze changes of the OH bands in more detail, we have fitted our spectra according to eq 1 where we have

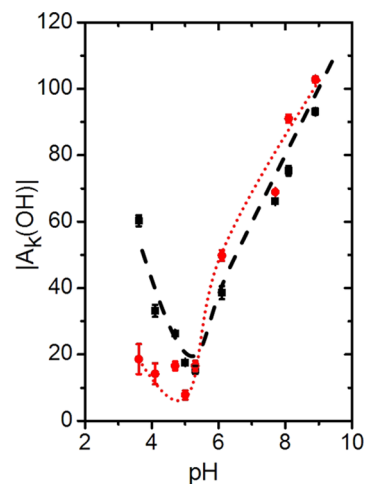


Figure 7. pH dependence of the amplitudes of the OH stretching vibration at 3200 (■) and 3450 cm^{-1} (red circle). The dotted lines guide the eye.

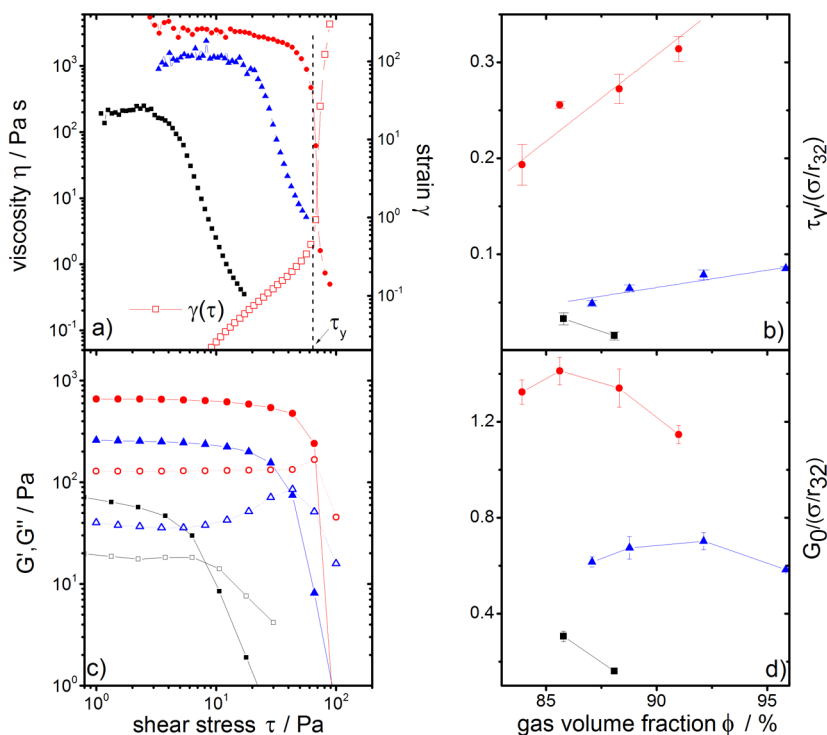


Figure 8. Steady and oscillatory shear ($f = 1$ Hz) measurements for BLG foams at different pH: ■, pH 3; red circle, pH 5; blue triangle, pH 6.8. (a) The viscosity η and (c) the moduli G' and G'' plotted as a function of applied stress τ at similar gas volume fractions ($\phi \approx 0.85$). The vertical dashed line in (a) shows the position of the yield stress that is derived from the strain versus stress graph $\gamma(\tau)$ as plotted exemplarily for pH 5 (open red square). (c) Apparent yield stress τ_y and (d) plateau value of the storage modulus G_0 in dependence of the gas volume fraction. Both quantities τ_y and G_0 are normalized by Laplace pressure (σ/r_{32}).

considered additional inhomogeneous broadening of the OH line shapes by convoluting the homogeneous (Lorentzian) lines by Gaussians. Figure 7 presents the oscillator strength A_k of OH bands as a function of pH. A pronounced decrease in the amplitude for pH ~ 5 with a subsequent increase is observed.

As the OH amplitudes are highly sensitive to the electric field induced by the charge of BLG, a minimum in the amplitudes around the IEP can be attributed to a minimum in protein charge and, consequently, to the interfacial point of zero net charge. For more acidic and alkaline pH, BLG carries a positive and negative net charge, respectively, which leads to a high orientation of the water dipoles. Crossing the point of zero net charge at the interface causes a change in the sign of E_{dc} and, hence, a change in net orientation of interfacial H_2O by 180° (Figure 6). The latter can be confirmed by the changes in polarity of the vibrational band around 3050 cm^{-1} which appears as positive going feature for pH < 5 and as a negative going feature for pH > 5 (Figure 5b). However, the origin of this apparent phase reversal lies not within net orientation of the BLG layer and its CH groups, but in the orientation of the interfacial H_2O , which can be easily orientated and polarized. In fact, changes in net orientation of interfacial H_2O lead pH < 5 to constructive interference conditions of the 3050 cm^{-1} band with the broad OH stretching band, while destructive interference at pH > 5 is observed. Obviously the net orientation of CH groups from the BLG layers does not change when the interfacial isoelectric point is crossed at pH 5; otherwise, the relative phase would not change and as consequence the appearance of the 3050 cm^{-1} band would be unchanged.

Obviously, the bulk isoelectric point at pH ~ 5.1 (Figure 1), the minimum in surface tension (Figure 2), the maximum in

storage modulus E' (Figure 3), and layer thickness (Figure 4) correspond to a minimum in the SFG amplitudes of the interfacial water molecules (Figure 7) that is indicative for zero net charge at the interface.

3.4. Rheology of Foams from β -Lactoglobulin Solutions. As the interfacial properties of the BLG layers can influence foam properties substantially,⁵⁴ measurements of the rheology of BLG foams were performed. The apparent yield stresses and the elastic moduli of the foams are presented in Figure 8. In Figure 8a, the flow curves of the BLG foams at similar gas volume fractions are shown. All curves exhibit the same characteristic features. At low stresses a very high constant apparent viscosity is measured before a sharp decrease appears that is coupled with the onset of foam flow. The point of yielding can be obtained by plotting the strain γ against the applied shear stress τ . The strain curve $\gamma(\tau)$ can be divided in two regions with different slopes: in the first region the slope is close to 1, and consequently, only very small deformations of the foam occur. In the second region the slope increases drastically, indicating flowing of the foam. Hence, the point of change in slope is determined as apparent yield stress. As can be seen in Figure 8b, the apparent yield stress is maximal for pH 5 followed by pH 6.8 and pH 3. The storage modulus G' (Figure 8c) stays constant at low stress amplitudes which is indicative for the linear viscoelastic regime. Videos show that in this range the bubble network can withstand the applied stress and the bubbles stay at their original positions. The end of the linear viscoelastic regime, where G' starts to decrease, is coupled with the yielding of the foam (see Figure 8a). Here, the gas bubbles of the foam start to move past each other. The pH dependence of the storage modulus is similar as for the yield

stress, giving the highest values at pH 5, followed by pH 6.8 and the lowest values for pH 3.

Figures 8b and 8d show that the described behavior of the foam is consistent over the whole range of measured gas volume fractions. In these graphs the yield stress and storage modulus are normalized by the Laplace pressure to account for the bubble sizes. Foams at pH 3 with $\phi > 88\%$ could not be generated due to a very high coalescence rate. For pH 6.8 and 5, $\tau_y/(\sigma/r_{32})$ increases linearly with the gas volume fraction. For $G_0/(\sigma/r_{32})$ there is no obvious ϕ dependence identifiable. In both cases this behavior of the BLG foams is different compared to the behavior of surfactant and casein foams where several studies^{55,56} report a quadratic increase of $\tau_y/(\sigma/r_{32})$ and G_0 with gas volume fraction.

To summarize the results of our foam rheology studies, the highest apparent yield stress and storage moduli can be found in foams from solutions with a pH close to the IEP of BLG. Obviously, the rheology of macroscopic foams is closely related to the properties of BLG modified air–water interfaces, e.g., the already discussed pH-dependent behavior of E' (Figure 3). Higher surface dilational moduli E' lead to higher foam stabilities, yield stresses, and storage moduli, which is in accordance with reported results.⁵⁷

4. GENERAL DISCUSSION

In order to understand the macroscopic behavior of foams from a microscopic picture of the ubiquitous air–water interface, we will now combine the above-discussed information on BLG interfacial layers with the rheological properties of macroscopic BLG foams.

Using interface analysis, we find that the solution pH can be used to tune the interaction potential of proteins at the air–water interface from a repulsive to an attractive regime. We have identified three pH regions where BLG carries either positive, negative, or zero net charge which results to substantial changes in the molecular structure of BLG adsorption layers.

At a pH near the IEP, the absence of net charge minimizes the electrostatic repulsion of proteins to a point where the protein–protein interaction becomes attractive. The latter allows the formation of multilayers with a dense BLG network with high interfacial dilational elasticity while protein charging leads to a decrease of interfacial dilational elasticity of the BLG layers as the elastic behavior of such layers is affected by the protein–protein interactions. The change from repulsive interaction for highly charged proteins to attractive interactions and the increased number density of BLG at the IEP account for the observed maximum in the interfacial dilational elasticity E' . Higher E' at the IEP hinder the foam from destabilization, drainage, and disproportionation as the increased E' decreases the rate of these destabilization mechanisms.⁵⁸ The network of BLG multilayers formed around the gas bubbles of the foam at the interfacial IEP increases therefore the foam stability. This network is beneficial to prevent foam drainage and coarsening⁶ and increases the resistance of the foam toward mechanical stress as was shown by our foam rheological measurements. The electrostatic repulsions among charged BLG molecules within the layers at pH <4 and pH >7 prevent the formation of multiple layers, and only a monolayer of BLG can exist at the interface. Consequently, the interfacial dilational elasticity together with the resistance to shear is decreasing with increasing repulsion between the BLG molecules.

Although the overall interfacial and macroscopic behaviors are very similar for pH values below and above the interfacial IEP, mechanical properties such as E' , G' , and τ_y are at pH 3 systematically smaller compared to pH 6.8 on the one hand. However, surface tension (Figure 2) and ellipsometry (Figure 4) show no differences between very acidic and basic pH with similar absolute values of the zeta potentials (Figure 1). It is now interesting to analyze the pH dependence of the SFG amplitude from OH stretching vibrations which is very sensitive to the local electric field. At a pH more acidic than the interfacial IEP, the 3200 cm^{-1} band is much more pronounced compared to more alkaline pH, which becomes even more obvious when the oscillator strength of the OH stretching bands in Figure 7 is analyzed. At pH 3.6 the oscillator strength of the band centered at 3200 cm^{-1} is ~ 60 arbitrary units while the amplitude of the 3450 cm^{-1} band is ~ 18 arbitrary units only. At pH of 7 the oscillator strengths of both bands are on a similar level of ~ 67 arbitrary units. Previously, the 3200 cm^{-1} band was attributed to a more ordered tetrahedrally coordinated network of hydrogen-bonded water molecules, while the 3450 cm^{-1} band was assigned to a more disordered network.⁵³ As the SFG intensity of OH stretching bands can be related to the local electric field that is generated by the adsorbed proteins at the interface, the observed intensity differences in the discussed pH regions can be related to different charging conditions. In fact, at pH 3 and 7 an overall charge of +20 e and -8 e, respectively, was calculated from the amino acid sequence and determined by titration, respectively.^{57,59} Consequently, the significantly higher charging of the interface at pH 3 compared to pH 7 leads to strong polar ordering of interfacial water molecules and much weaker contributions from disordered water molecules to the SFG intensity. Therefore, the SFG intensity of the 3200 cm^{-1} band due to tetrahedrally coordinated H_2O is much higher than the intensity of the 3450 cm^{-1} band due disordered interfacial water molecules. The situation at pH 7 changes as the local electric field is weaker and results in an increase of the SFG contributions from less ordered water molecules. Regarding the charge effects, it is interesting to note that our zeta potential measurements of the bulk BLG do not resolve differences in the protein net charge between pH 3 and pH 7, which seemingly contradicts our conclusions from SFG spectra. However, the zeta potential is determined from electrophoretic mobility measurements where the electric potential at the slipping plane is probed. Here, ions that migrate with the protein are separated from ions not migrating with the protein in the electric field. What seems to be more important is the charge (distribution) directly at the protein surface. The difference between SFG data and zeta potential at acidic pH and the comparison with the estimated charge of BLG indicate that SFG probes the field in the compact double layer close to the protein surface and that the zeta potential is obviously modified by charge screening within the compact double layer (see also below).

For pH values where only a monolayer of BLG is established at the air–water interface, changes in surface charging do not lead to noticeable changes in the coverage of BLG at the air–water interface but rather influence the intermolecular interactions and thus the interfacial elasticity. As the higher local electric field at pH 3 leads to stronger electrostatic repulsions within BLG layers, systematically lower values in E' , G' , and τ_y are not surprising but are consistent with the change in interaction potential of interfacial proteins which determines

these rheological properties. Our results from foam rheology measurements show a clear difference in foam stability at pH 3 and pH 6.8, which might not only be affected by the discussed electrostatic effects directly at the protein surface: As already mentioned, our measurements of the surface tension (Figure 2) do not show a difference between acidic and basic pH at comparatively low BLG concentrations. Since the pH is adjusted by adding diluted HCl or NaOH to the BLG solutions, the ionic strength of the resulting electrolyte is pH dependent. At a pH of 3 the ionic strength is necessarily higher compared to a pH near 7. As a consequence, the higher surface charge at pH 3 and thus the electrostatic repulsion will be partially screened by additional ions in the electric double layer, which also shrinks in its size as the Debye length decreases with increasing ionic strength. This charge screening is higher for pH 3 compared to pH 7 and presumably results into very similar intermolecular interactions at these pH values outside the compact double layer. In fact, this conclusion is corroborated by our observation of an identical absolute value of the zeta potential (Figure 1)—the potential at the shear plane—and similar surface tensions (Figure 2) as well as layer thicknesses (Figure 4).

By increasing the BLG concentration for our foam rheology measurements, this effect is even intensified as more HCl needs to be added in order to adjust the pH to a value of 3. As shown in Table 1, the surface tension is then smaller at pH 3 compared to pH 6.8. The rheology of BLG layers at the air–water interface and macroscopic BLG foams is, however, also dependent on the composition of the entire interfacial layer that includes BLG proteins, solvating water molecules, and ions which stabilize the charged layer at interface. Crossing the isoelectric point will necessarily lead to substantial changes in the electric double layer around the proteins, which is also influenced by the ionic strength (see above). For that reason, differences in foam rheology and surface dilational rheology are not surprising for pH values of 3 and 7.

In addition to the discussed pH-dependent properties of the interfacial layer, it is interesting to discuss also possible structural changes of the BLG molecule that might occur at different pH. In fact, in their NMR study Molinari et al. report that at acidic pH the conformation of BLG is likely to consist of a stable core together with disordered regions.⁶⁰ Furthermore, a buried hydrophobic cluster was identified, and it was suggested that this cluster leads to high structural stability of BLG at acidic pH⁶¹ which is consistent with thermodynamic studies.⁶² In addition to these observations, Shimizu et al.⁶³ found a clear increase in hydrophobicity from pH 7 to 3 that is accompanied by decreased foam stability.⁵⁷ Taking the latter observations into account, an increase in hydrophobicity might result into a protein layer with the molecules protruding farther into the air phase which then will lead necessarily to weaker screening of the BLG surface charges as less water molecules and ions can be involved into the stabilization of the charged layer. Hence, repulsive interaction within the BLG layer increases.

5. SUMMARY AND CONCLUSION

In this study we have addressed macroscopic properties of aqueous β -lactoglobulin (BLG) foams and the molecular properties of BLG modified air–water interfaces which are inherently connected to the macroscopic foam as they constitute its major structural element. For that purpose we have applied a unique combination of foam rheology measurements and interfacial sensitive methods such as sum-

frequency generation, ellipsometry, bubble profile analysis tensiometry, and surface dilational rheology.

We identify three regions of different pH, where both macroscopic and microscopic properties change quite dramatically and are interconnected. At pH conditions around 5—which we identify as the isoelectric point of the interface—interfacial layers of BLG carry no net charge and exhibit attractive intermolecular interactions. The latter causes the formation of disordered and presumably agglomerated BLG multilayers, resulting in a maximum in the surface coverage of BLG. For increasingly alkaline and acidic pH conditions the protein–protein interactions change from attractive to a highly repulsive regime that leads to a formation of BLG monolayers and to highly polar ordered water molecules. Changes in layer thickness and protein–protein interaction (attractive or repulsive) are shown to dramatically change the interfacial dilational elasticity E' which exhibits a maximum around pH 5 where multilayers with zero net charge exists at the air–water surface. This molecular information was correlated with the behavior of the macroscopic BLG foam. Thick and disordered adsorption layers lead to highest foam stability and maximum yield stress as the gas bubbles are protected by the proteins arranged around them. Thin and more ordered layers with strong electrostatic repulsions show a significantly decreased resistance to mechanical stress that is strongly influenced by the actual net charge on the protein surface.

AUTHOR INFORMATION

Corresponding Author

*E-mail: Bjoern.Braunschweig@lfg.fau.de.

Notes

The authors declare no competing financial interest.

ACKNOWLEDGMENTS

The authors thank the group of Ulrich Kulozik (Technische Universität München, Germany) for the supply of high quality β -lactoglobulin.

K.E., C.K., B.B., and W.P. gratefully acknowledge the funding by the German National Science Foundation (DFG) through the Leibniz program and the DFG-AiF cluster project on “Protein Foams” project PE427/21-1. G.G. and R.M. as well as M.L. and N.W. acknowledge also the funding by the DFG-AiF cluster project on “Protein Foams” Mi418/20-1 and Wi 3138/10-1.

REFERENCES

- (1) Lefebvre, L.-P.; Banhart, J.; Dunand, D. C. Porous metals and metallic foams: current status and recent developments. *Adv. Eng. Mater* **2008**, *10*, 775–787.
- (2) Fameau, A.-L.; Saint-Jalmes, A.; Cousin, F.; Houinsou Houssou, B.; Novales, B.; Navailles, L.; Nallet, F.; Gaillard, C.; Boué, F.; Douliez, J.-P. Smart foams: switching reversibly between ultrastable and unstable foams. *Angew. Chem.* **2011**, *123*, 8414–8419.
- (3) Prud'homme, R. K.; Khan, S. A. *Foams: Theory, Measurements, and Applications*; Marcel Dekker, Inc.: New York, 1996.
- (4) Mezzenga, R.; Schurtenberger, P.; Burbidge, A.; Michel, M. Understanding foods as soft materials. *Nat. Mater.* **2005**, *4*, 729–740.
- (5) Foegeding, E. A.; Luck, P. J.; Davis, J. P. Factors determining the physical properties of protein foams. *Food Hydrocolloids* **2006**, *20*, 284–292.
- (6) Engelhardt, K.; Rumpel, A.; Walter, J.; Dombrowski, J.; Kulozik, U.; Braunschweig, B.; Peukert, W. Protein adsorption at the electrified air–water interface: implications on foam stability. *Langmuir* **2012**, *28*, 7780–7787.

- (7) Dickinson, E.; Ettelaie, R.; Murray, B. S.; Du, Z. Kinetics of disproportionation of air bubbles beneath a planar air-water interface stabilized by food proteins. *J. Colloid Interface Sci.* **2002**, *252*, 202–213.
- (8) Davis, J. P.; Foegeding, E. A. Foaming and interfacial properties of polymerized whey protein isolate. *J. Food Sci.* **2004**, *69*, C404.
- (9) McClellan, S. J.; Franses, E. I. Effect of concentration and denaturation on adsorption and surface tension of bovine serum albumin. *Colloids Surf., B* **2003**, *28*, 63–75.
- (10) Lu, J. R.; Su, T. J.; Penfold, J. Adsorption of serum albumins at the air/water interface. *Langmuir* **1999**, *15*, 6975–6983.
- (11) Atkinson, P. J.; Dickinson, E.; Horne, D. S.; Richardson, R. M. Neutron reflectivity of adsorbed β -casein and β -lactoglobulin at the air/water interface. *J. Chem. Soc., Faraday Trans.* **1995**, *91*, 2847–2854.
- (12) Richter, A. G.; Kuzmenko, I. Using in situ X-ray reflectivity to study protein adsorption on hydrophilic and hydrophobic surfaces: benefits and limitations. *Langmuir* **2013**, *29*, 5167–5180.
- (13) Stocco, A.; Drenckhan, W.; Rio, E.; Langevin, D.; Binks, B. P. Particle-stabilised foams: an interfacial study. *Soft Matter* **2009**, *5*, 2215–2222.
- (14) Miller, R.; Fainerman, V. B.; Wüstneck, R.; Krägel, J.; Trukhin, D. V. Characterisation of the initial period of protein adsorption by dynamic surface tension measurements using different drop techniques. *Colloids Surf., A* **1998**, *131*, 225–230.
- (15) Bouyer, E.; Mekhloufi, G.; Huang, N.; Rosilio, V.; Agnely, F. β -Lactoglobulin, gum arabic, and xanthan gum for emulsifying sweet almond oil: formulation and stabilization mechanisms of pharmaceutical emulsions. *Colloids Surf., A* **2013**, *433*, 77–87.
- (16) Zhang, C.; Myers, J. N.; Chen, Z. Elucidation of molecular structures at buried polymer interfaces and biological interfaces using sum frequency generation vibrational spectroscopy. *Soft Matter* **2013**, *9*, 4738–4761.
- (17) Roke, S. Nonlinear optical spectroscopy of soft matter interfaces. *ChemPhysChem* **2009**, *10*, 1380–1388.
- (18) Wang, J.; Buck, S. M.; Chen, Z. Sum frequency generation vibrational spectroscopy studies on protein adsorption. *J. Phys. Chem. B* **2002**, *106*, 11666–11672.
- (19) Kim, G.; Gurau, M.; Kim, J.; Cremer, P. S. Investigations of lysozyme adsorption at the air/water and quartz/water interfaces by vibrational sum frequency spectroscopy. *Langmuir* **2002**, *18*, 2807–2811.
- (20) Fu, L.; Ma, G.; Yan, E. C. Y. In situ misfolding of human islet amyloid polypeptide at interfaces probed by vibrational sum frequency generation. *J. Am. Chem. Soc.* **2010**, *132*, 5405–5412.
- (21) Liu, Y.; Jasensky, J.; Chen, Z. Molecular interactions of proteins and peptides at interfaces studied by sum frequency generation vibrational spectroscopy. *Langmuir* **2012**, *28*, 2113–2121.
- (22) Ding, B.; Soblosky, L.; Nguyen, K.; Geng, J.; Yu, X.; Ramamoorthy, A.; Chen, Z. Physiologically-relevant modes of membrane interactions by the human antimicrobial peptide, LL-37, revealed by SFG experiments. *Sci. Rep.* **2013**, *3*, 1854.
- (23) Thennarasu, S.; Huang, R.; Lee, D.-K.; Yang, P.; Maloy, L.; Chen, Z.; Ramamoorthy, A. Limiting an antimicrobial peptide to the lipid-water interface enhances its bacterial membrane selectivity: a case study of MSI-367. *Biochemistry* **2010**, *49*, 10595–10605.
- (24) Toro-Sierra, J.; Tolkach, A.; Kulozik, U. Fractionation of α -Lactalbumin and β -Lactoglobulin from whey protein isolate using selective thermal aggregation, an optimized membrane separation procedure and resolubilization techniques at pilot plant scale. *Food Bioprocess. Technol.* **2013**, *6*, 1032–1043.
- (25) Wit, J. N. de Thermal behaviour of bovine β -lactoglobulin at temperatures up to 1500°C. a review. *Trends Food Sci. Technol.* **2009**, *20*, 27–34.
- (26) Loglio, G.; Pandolfini, P.; Miller, R.; Makievski, A.; Ravera, F.; Ferrari, M.; Liggieri, L. Drop and bubble shape analysis as tool for dilational rheology studies of interfacial layers. In *Novel Methods to Study Interfacial Layers*, 1st ed.; Möbius, D., Miller, R., Eds.; Elsevier: Amsterdam, 2001.
- (27) Wüstneck, R.; Fainerman, V. B.; Aksenenko, E. V.; Kotsmar, C.; Pradines, V.; Krägel, J.; Miller, R. Surface dilatational behavior of β -casein at the solution/air interface at different pH values. *Colloids Surf., A* **2012**, *404*, 17–24.
- (28) Gochev, G.; Retzlaff, I.; Aksenenko, E. V.; Fainerman, V. B.; Miller, R. Adsorption isotherm and equation of state for β -Lactoglobulin layers at the air/water surface. *Colloids Surf., A* **2013**, *422*, 33–38.
- (29) Benjamins, J.; Lucassen-Reynder, E. H. Interfacial rheology of adsorbed protein layers. In *Interfacial Rheology*; Liggieri, L., Miller, R., Krotov, V. V., Eds.; Brill: Leiden, 2009.
- (30) Holt, S. A.; White, J. W. The molecular structure of the surface of commercial cow's milk. *Phys. Chem. Chem. Phys.* **1999**, *1*, 5139–5145.
- (31) Marsh, R. J.; Jones, R. A. L.; Sferrazza, M.; Penfold, J. Neutron reflectivity study of the adsorption of β -Lactoglobulin at a hydrophilic solid/liquid interface. *J. Colloid Interface Sci.* **1999**, *218*, 347–349.
- (32) Verheul, M.; Pedersen, J. S.; Roefs, S. P. F. M.; Kruij, K. G. de Association behavior of native β -lactoglobulin. *Biopolymers* **1999**, *49*, 11–20.
- (33) Shen, Y. R. *The Principles of Nonlinear Optics*; John Wiley & Sons: New York, 1984.
- (34) Rumpel, A.; Novak, M.; Walter, J.; Braunschweig, B.; Halik, M.; Peukert, W. Tuning the molecular order of C60 functionalized phosphonic acid monolayers. *Langmuir* **2011**, *27*, 15016–15023.
- (35) Wierenga, P. A.; Gruppen, H. New views on foams from protein solutions. *Curr. Opin. Colloid Interface Sci.* **2010**, *15*, 365–373.
- (36) Nino, M. R.; Sanchez, C. C.; Fernandez, M. C.; Patino, J. M. Protein and lipid films at equilibrium at air-water interface. *J. Am. Oil Chem. Soc.* **2001**, *78*, 873–879.
- (37) Feitosa, K.; Marze, S.; Saint-Jalmes, A.; Durian, D. Electrical conductivity of dispersions: from dry foams to dilute suspensions. *J. Phys.: Condens. Matter* **2005**, *17*, 6301.
- (38) Chi, E. Y.; Krishnan, S.; Randolph, T. W.; Carpenter, J. F. Physical stability of proteins in aqueous solution: mechanism and driving forces in nonnative protein aggregation. *Pharm. Res.* **2003**, *20*, 1325–1336.
- (39) Fennema, O. R. *Food Chemistry*, 3rd ed.; Marcel Dekker: New York, 1996.
- (40) Wong, D. W. S.; Camirand, W. M.; Pavlath, A. E.; Parris, N.; Friedman, M. Structures and functionalities of milk proteins. *Crit. Rev. Food Sci. Nutr.* **1996**, *36*, 807–844.
- (41) Bhandari, B.; Roos, Y. H., Eds.; *Food Materials Science and Engineering*; Wiley-Blackwell: Ames, IA, 2012.
- (42) Mucha, M.; Frigato, T.; Levering, L. M.; Allen, H. C.; Tobias, D. J.; Dang, L. X.; Jungwirth, P. Unified molecular picture of the surfaces of aqueous acid, base, and salt solutions. *J. Phys. Chem. B* **2005**, *109*, 7617–7623.
- (43) Dickinson, E. Proteins at interfaces and in emulsions stability, rheology and interactions. *J. Chem. Soc., Faraday Trans* **1998**, *94*, 1657–1669.
- (44) Wüstneck, R.; Krägel, J.; Miller, R.; Fainerman, V. B.; Wilde, P. J.; Sarker, D. K.; Clark, D. C. Dynamic surface tension and adsorption properties of β -casein and β -lactoglobulin. *Food Hydrocolloids* **1996**, *10*, 395–405.
- (45) Perriman, A. W.; Henderson, M. J.; Holt, S. A.; White, J. W. Effect of the air–water interface on the stability of β -Lactoglobulin. *J. Phys. Chem. B* **2007**, *111*, 13527–13537.
- (46) Beretta, S.; Chirico, G.; Baldini, G. Short-range interactions of globular proteins at high ionic strengths. *Macromolecules* **2000**, *33*, 8663–8670.
- (47) Majhi, P. R.; Ganta, R. R.; Vanam, R. P.; Seyrek, E.; Giger, K.; Dubin, P. L. Electrostatically driven protein aggregation: β -Lactoglobulin at low ionic strength. *Langmuir* **2006**, *22*, 9150–9159.
- (48) Gottschalk, M.; Nilsson, H.; Roos, H.; Halle, B. Protein self-association in solution: the bovine β -lactoglobulin dimer and octamer. *Protein Sci.* **2003**, *12*, 2404–2411.
- (49) Wang, J.; Buck, S. M.; Chen, Z. The effect of surface coverage on conformation changes of bovine serum albumin molecules at the air-solution interface detected by sum frequency generation vibrational spectroscopy. *Analyst* **2003**, *128*, 773–778.

(50) Chen, X.; Flores, S. C.; Lim, S.-M.; Zhang, Y.; Yang, T.; Kherb, J.; Cremer, P. S. Specific anion effects on water structure adjacent to protein monolayers. *Langmuir* **2010**, *26*, 16447–16454.

(51) Chen, X.; Yang, T.; Kataoka, S.; Cremer, P. S. Specific ion effects on interfacial water structure near macromolecules. *J. Am. Chem. Soc.* **2007**, *129*, 12272–12279.

(52) Richmond, G. L. Molecular bonding and interactions at aqueous surfaces as probed by vibrational sum frequency spectroscopy. *Chem. Rev.* **2002**, *102*, 2693–2724.

(53) Shen, Y. R.; Ostroverkhov, V. Sum-frequency vibrational spectroscopy on water interfaces: polar orientation of water molecules at interfaces. *Chem. Rev.* **2006**, *106*, 1140–1154.

(54) Georgieva, D.; Cagna, A.; Langevin, D. Link between surface elasticity and foam stability. *Soft Matter* **2009**, *5*, 2063–2071.

(55) Marze, S.; Guillermic, R. M.; Saint-Jalmes, A. Oscillatory rheology of aqueous foams: surfactant, liquid fraction, experimental protocol and aging effects. *Soft Matter* **2009**, *5*, 1937–1946.

(56) Mason, T. G.; Bibette, J.; Weitz, D. A. Elasticity of compressed emulsions. *Phys. Rev. Lett.* **1995**, *75*, 2051–2054.

(57) Davis, J. P.; Foegeding, E. A.; Hansen, F. K. Electrostatic effects on the yield stress of whey protein isolate foams. *Colloids Surf., B* **2004**, *34*, 13–23.

(58) van Prins, A. B. M.; Boerboom, F.; Kalsbeek, H. Relation between surface rheology and foaming behavior of aqueous protein solutions. In *Proteins at liquid interfaces*; Miller, R., Möbius, D., Eds.; Elsevier: Amsterdam, 1998.

(59) Nozaki, Y.; Bunville, L. G.; Tanford, C. Hydrogen ion titration curves of β -lactoglobulin. *J. Am. Chem. Soc.* **1959**, *81*, 5523–5529.

(60) Molinari, H.; Ragona, L.; Varani, L.; Musco, G.; Consonni, R.; Zetta, L.; Monaco, H. L. Partially folded structure of monomeric bovine β -lactoglobulin. *FEBS Lett.* **1996**, *381*, 237–243.

(61) Ragona, L.; Pusterla, F.; Zetta, L.; Monaco, H. L.; Molinari, H. Identification of a conserved hydrophobic cluster in partially folded bovine β -lactoglobulin at pH 2. *Folding Des.* **1997**, *2*, 281–290.

(62) Kella, N. K.; Kinsella, J. E. Enhanced thermodynamic stability of beta-lactoglobulin at low pH. A possible mechanism. *Biochem. J.* **1988**, *255*, 113–118.

(63) Shimizu, M.; Saito, M.; Yamauchi, K. Emulsifying and structural properties of beta-lactoglobulin at different pHs. *Agric. Biol. Chem.* **1985**, *49*, 189–194.